ACS OMEGA

http://pubs.acs.org/journal/acsodf

Article

Heat Transfer Characteristics of Fullerene and Titania Nanotube Nanofluids under Agitated Quench Conditions

Jaimon Dennis Quadros,* Sher Afghan Khan, Prashanth T, Yakub Iqbal Mogul, Hanumanthraya R, Mohamed Abbas, C. Ahamed Saleel, and Saboor Shaik*

Cite This: *ACS Omega* 2022, 7, 47764−47783

Read Online

ACCESS | Metrics & More | Article Recommendations

ABSTRACT: Distilled water and aqueous fullerene nanofluids having concentrations of 0.02, 0.2, and 0.4 vol % and titania (titanium dioxide, TiO_2) nanofluids of 0.0002, 0.002, and 0.02 vol % were analyzed for heat transfer characteristics. Quenching mediums were stirred at impeller speeds of 0, 500, 1,000, and 1,500 RPMs in a typical Tensi agitation system. During the quenching process, a metal probe made of ISO 9950 Inconel was used to record the temperature history. The inverse heat conduction method was used to calculate the spatial and temporal heat flux. The nanofluid rewetting properties were measured and matched to those of distilled water. The maximum mean heat flux was 3.26 MW/m^2, and the quickest heat extraction was 0.2 vol % fullerene nanofluid, according to the results of the heat transfer investigation.

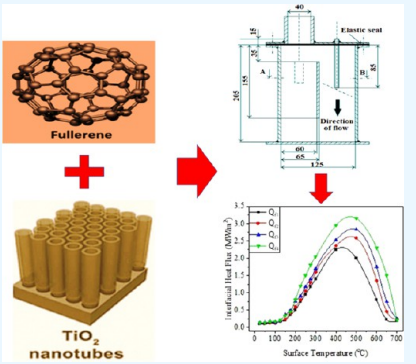

1. INTRODUCTION

The industrial procedure of quench hardening is employed to reinforce metal alloys. Austenitization temperature (usually above 860 °C) and quick cooling in a heat transfer medium is used to harden steels. As a general rule, liquid quenching media are favored over gaseous and solid media because they are significantly faster and more efficient in transferring heat. Hardened steel quenching was done using water during the early stages of quenching technology. This was because it was readily available and inexpensive. It was established, however, that quenching with water was a drawback due to its inability to wet the surface of the metal uniformly. High alloys and steels of intricate shapes could not be quenched hardened using water because of higher quench severity. Increasing water temperature was intended to reduce or eliminate these defects that generated uneven cooling at low temperatures between 300 and 200 °C in the metal. This resulted in soft areas, deformation, and warping concerns with increased intensity.[1]

Dispersing nanoparticles (1 to 100 nm) of solid materials in base fluids produces nanofluids and heat transport mediums. Nonmetallic materials such as copper, titanium, multiwall carbon nanotubes (MWCT), and silicon carbides can be used to create a variety of nanofluids.[2] During quenching, the quenchant's capacity to remove heat from the hot surface of the metal is assessed. There was no noticeable difference in the cooling rates of water and nanofluids when the nanoparticle concentrations were low. Particles were deposited on the quench probe using nanoparticles, namely, water-based silica, alumina, and diamond.[3] According to Ciloglu and Bolukbasi, deposition influences the cooling rate during quenching.[4] According to Schauperl et al., nanofluids with 0.2 g/L of nanoparticles under unagitated quench conditions showed a significant improvement in the optimal heat transfer coefficient over their base fluids (water and PAG solution, 5, 10, and 20 vol %).[5] These investigations demonstrate the film boiling stage shortening, indicating that the cooling metal surface gets wet earlier. 304L SS probes were quenched with carbon nanotube (CNT) nanofluids, as demonstrated by Babu and Kumar, who found a greater maximum heat flux at a bath temperature of 40 °C.[6] According to the researchers, the increasing random mobility of water particles accounted for the rise in the peak heat flux. The peak heat flux was reduced while quenching new probes in water−clay nanofluids of varying concentrations.[7] When constructing a nanoquenchant, it is critical to choose the right material type for the purpose. Deionized water was used to control the heat transfer properties of the copper nanofluid quench medium of concentration 2.6 mg/L, produced by laser ablation. Improved cooling rates for the nanofluid were observed for agitation rates of 0, 390, 850, and 1170 rpm when compared to water at 0 rpm, lower at 390 rpm, and similar at 850 and 1170 RPMs,

Received: August 22, 2022
Accepted: November 24, 2022
Published: December 12, 2022

https://doi.org/10.1021/acsomega.2c05397
ACS Omega 2022, 7, 47764−47783

respectively.[8] Heat transfer characteristics of the chemically treated CNT nanofluid were examined at agitation rates of 1000 and 1600 RPMs using a vane-type mechanical stirrer.[6] The nanofluid's peak heat flux and heat extraction capabilities decreased by approximately 30 and 22% for the 1600 and 1000 rpm impeller speeds, respectively. Based on a study by Afzal et al., the impact of ultrasonication duration and surfactants on the ZnO and CuO nonfluids was investigated. Through experiments, a stable ZnO nanofluid was prepared using the eriochrome black T and olylamine surfactants, while the CuO nanofluid stabilized using the olylamine surfactant alone. It was found that the ultrasonication time increased from 2 to 8 h, and the stability of ZnO with the eriochrome black T nanofluid was higher when compared to the other nanofluids.[9] Wlazlak et al. determined the thermal performance of thermosyphon filled with the graphene oxide (GO) nanofluid. The study focused on the deterioration of particles, surfactant presence, and working conditions. The study revealed that the GO nanofluid showed enhanced heat transfer at lower heat loads; these improvements were restricted to the evaporator section.[10] Saleh et al. investigated the CO_2 emissions of the Al_2O_3/water nanofluid in a flat plate solar collector. The experiments were performed for the volume loading of 0.1, 0.2, and 0.3% and volume flow rates ranging from 120 to 300 L/h. Results showed that the thermal efficiency of the collector increased with the increase in both particle volume loadings and volume flow rates.[11] Afzal et al. investigated the heat transfer characteristics of MWCNT in rectangular channels. The convective heat transfer coefficient (h) for the MWCNT−water nanofluid is compared with water for flow rates of 0.25, 0.5, and 0.75 L/min. It was observed that the h and actual heat transfer rate were found to be maximum for the flow rate of 0.5 L/min when compared to the other flow rates.[12] Samylingam et al. formulated a new heat transfer fluid of MXene (Ti_3C_2) suspended in pure olien palm oil (OPO) and investigated its thermal and energy performance in a hybrid solar thermal system. The MXene−OPO was prepared with loading concentrations of 0.01, 0.03, 0.05, 0.08, 0.1, and 0.2 wt %. The experimental results showed that a 0.2 wt % loading concentration yielded a 69% increase in thermal conductivity. Furthermore, around 61% reduction in viscosity was also observed for a temperature rise of 25 to 50 °C for nanofluids with 0.2 wt % of MXene.[13]

Based on the literature, most research on nanofluids emphasized CNT and graphene-based nanofluids. Similarly, fullerene is a carbon allotrope that exists as carbon spheres, but unlike graphene, it has a three-dimensional structure with excellent heat transfer properties. Titanium dioxide nanotubes are a nanoscale type of titanium oxide with a comparable structure and characteristics to CNT, making them perfect for usage in solutions and semiconductor thin films in optics, electronics, transistors, and energy storage. The goal of this study is, therefore, to determine (i) the measure of the spatial and temporal heat flux using the inverse heat conduction method, (ii) the wetting behavior of nanofluids and its effects on the uniformity with which heat is removed from the surface, and (iii) to obtain and test a quench media that improves the mechanical characteristics of steel during the quenching process, determined by experimenting with aqueous nanofluids under agitation and comparing the results to those obtained using distilled water as a quench medium. Aqueous fullerene and TNT solutions of varying concentrations were generated using the two-step approach in this study. The temperature, viscosity, density, and surface tension of nanofluids were measured, and the distribution of nanofluid droplets on an Inconel substrate was also investigated.

2. EXPERIMENTAL DETAILS

2.1. Nanofluid Preparation. A two-step preparation of the nanofluids was employed. Nanoparticles were obtained

Table 1. Information Regarding Quench Media

s.i. no.	nanoparticles	size	concentrations (vol %)	preparation technique
1.	distilled water			
2.	titanium dioxide (TiO_2) nanotube (TNT)	500 nm	0.0002 0.002 0.02	a mechanical mixing technique was employed, and a hand-held stirrer was used.
3.	fullerene	2−4 nm thick	0.02 0.2 0.4	ultrasonication for 40 kHz for 45 min

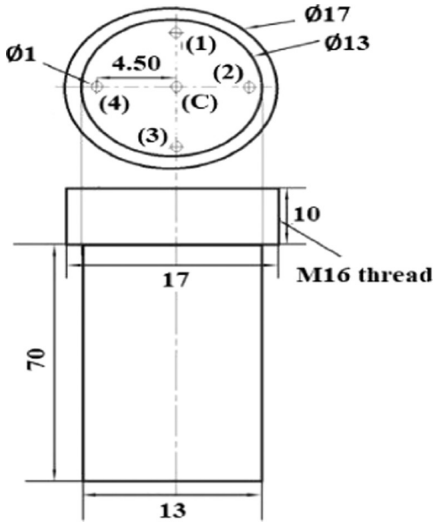

Figure 1. Inconel quench probe design.

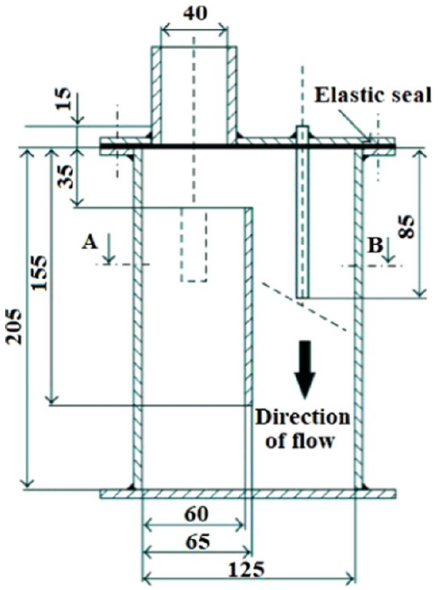

Figure 2. Geometry of the Tensi agitator.

https://doi.org/10.1021/acsomega.2c05397
ACS Omega 2022, 7, 47764−47783

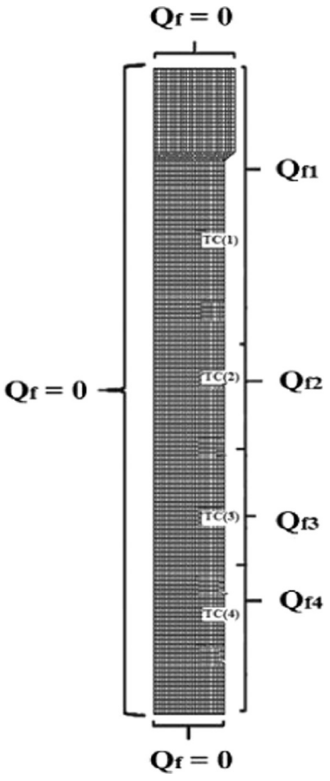

Figure 3. Meshed model of the quench probe.[16]

from commercial vendors and then dispersed in water using the two-step procedure. TNT was obtained as a paste, whereas fullerene was obtained as a powder. Table 1 contains information on the nanofluid media and how they were prepared.

2.2. Details of Quench Probe. Figure 1 illustrates a schematic drawing of quench probes identifying thermocouple positions. An investigation made of Inconel 600 alloys was used to determine the cooling properties of the quench media.

The probe was machined according to the ISO 9950 standard (⌀13 × 60 mm^2) specifications. To facilitate the ⌀1.0 mm K-type thermocouples for temperature measurement, the metal probe was drilled to create openings of 1.0 mm diameter. The Inconel probe is equipped with a 10 mm screw segment for attachment with the connecting pipe. The piping entirely blocks the entrance of the liquid medium into the drilled holes and allows the lateral quenching of the probe.

2.3. Details of the Agitation System. The quench tests were conducted under agitation using a Tensi agitation system, as illustrated in Figure 2. An electric furnace was used to preheat the Inconel probe encompassed in a thermocouple to about 850 °C before being transferred to the Tensi agitation system. K-type cables were used to connect the data acquisition system (DAQ, NI 9213) to the cold junction of the thermocouples. The DAQ was connected to a computer to capture the temperature history of the quenching process. The Tensi system consisted of a plexiglass quench tank that contained 1.5 L of the quench medium, the dimensions of which are shown in Figure 2. Agitation was carried out using a four-bladed propeller. Three propeller speeds of 0, 500, 1000, and 1500 rpm were used for quench experiments. The quenching process was carried out by positioning the system close to the furnace such that the probe is conveniently shifted from the furnace onto the Tensi quench tank. The surface temperature of the probe, as recorded by the near-surface sensors, was reduced by around 10 to 15 °C throughout the transfer. One of the near-surface sensors achieved a temperature of about 825 °C during the quenching of the hot probe in the liquid medium. The initial temperature of the quenching medium during the quenching process was 28 ± 3 °C, and the impeller was triggered before immersing in the hot probe. The temperature data was taken at intervals of 0.1 s, and the probe was cleaned with water and acetone following every cycle. The temperature and heat flux data recordings were reliable within 2% and reproducible inside 3%, despite oscillations developed by the impeller speeds.

2.4. Viscosity, Thermal Conductivity, and Density Measurement. A programmable rheometer Brookfield DV-III developed by Brookfield Engineering Laboratories was used to measure the quench medium viscosity. The ultralow adapter (ULA) accessory was used to measure water viscosity and nanofluids. The spindle was dipped into a specially developed sample container holding 16 mL of test liquid to determine the viscosity. Apparently, many parameters such as particle size and shape, solvent type, hydrogen bonding, temperature, base fluids, and alignment affect the thermal conductivity of nanofluids.[14] A Decagon-made KD2-Pro analyzer measured the thermal conductivity of nanofluids. The measurements were taken by immersing the sensor into a beaker that contained a 90 mL nanofluid medium. The weight displacement technique was implemented to measure the density of the quench media. For this purpose, a 50 mL specific gravity container was employed.

2.5. Interfacial Heat Flux Transients. The interface at the metal and quenchant are subject to spatiotemporal heat flux transients estimated using the near-surface thermocouple data via the inverse heat conduction approach. The thermal characteristics of the Inconel probe, along with the solution methods, were performed to determine the interfacial spatiotemporal heat flux.[15] The two-dimensional (2-D) model of the quench probe is shown in Figure 3. Heat flux transients at the boundary were measured using this model. The model was meshed evenly using four-node quadrilateral elements. Temperature measurements from quenching experiments were used as input to the model at nodes corresponding to locations, as shown in Figure 1. The Inconel probe model is comprised of four representations, namely, TC (1), TC (2), TC (3), and TC (4), that record the temperature values at a depth of 16, 32, 48, and 52 mm, respectively. The model mesh had 3500 elements. Four boundary heat flux sections were incorporated into the Inconel probe model. The convergence criteria were set to 10^{-6} in the Gauss−Siedel iterations.

2.6. Surface Tension and Contact Angle Measurements. The literature has noticed that wetting the quench medium on the surface of the probe has a stimulating effect on the cooling process. A KRUSS shape analyzer of DSA100S was used to investigate the droplet's spreading behavior and contact angle. A droplet of quench medium was dispensed onto the substrate using a 1 mL surgical syringe with a 0.5 mm diameter needle. A precision pump controlled the supply of droplet dispersion. The droplet dispersion phenomenon on the metal substrate was captured with a high-speed camera operating at 25 frames per second and analyzed using the KRUSS program. The software was installed with a curve fitting technique that measured the contact angle of the dispensed droplet. A needle with a diameter of 1.8 mm was attached to the syringe to determine the surface tension. A

https://doi.org/10.1021/acsomega.2c05397
ACS Omega 2022, 7, 47764−47783

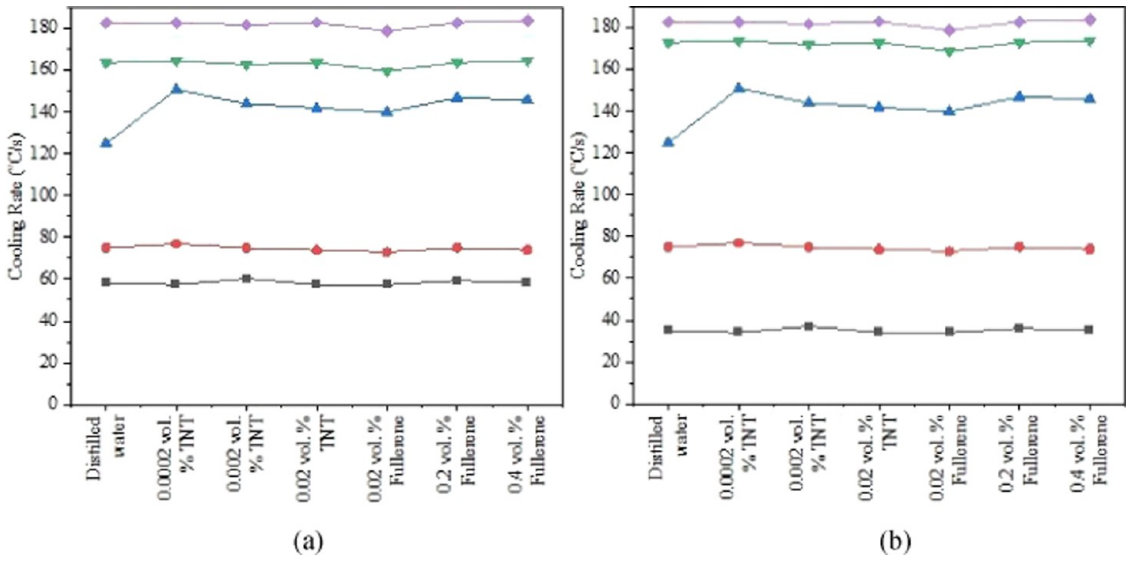

Figure 4. Variation of cooling rates with respect to distilled water, 0.0002, 0.002, and 0.02 vol % titania (titanium dioxide, TiO_2), and 0.02, 0.2, and 0.4 vol % fullerene nanofluids for different critical cooling temperatures (CR) of max, 700, 500, 300, and 200 under (a) still and (b) 500 rpm impeller speeds.

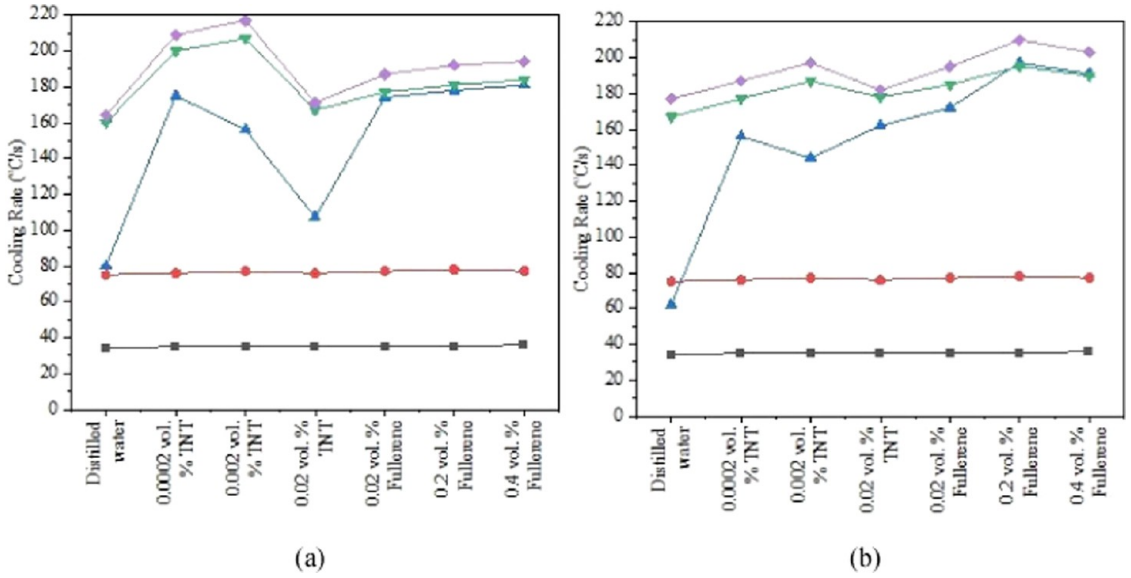

Figure 5. Variation of cooling rates with respect to distilled water, 0.0002, 0.002, and 0.02 vol % titania (titanium dioxide, TiO_2), and 0.02, 0.2, and 0.4 vol % fullerene nanofluids for different critical cooling temperatures (CR) of max, 700, 500, 300, and 200 under (a) 1000 and (b) 1500 rpm impeller speeds.

pendant of the quench medium was prepared and strung from the needle's tip to collect data. The density and viscosity of the liquid given as critical inputs to the Advance program were utilized to calculate the surface tension. Throughout the studies, the ambient temperature was fixed at 27 °C. Advance software was used to analyze the recorded images to determine the dynamic contact angle.

3. RESULTS AND DISCUSSION

The cooling rates, as per Figures 4 and 5, show that a vapor phase is initially generated as the Inconel probe is quenched in water and nanofluids, accompanied by nucleate boiling and convective cooling in the later stages.[16] During the commencement of quenching, the probe is engulfed by the vapor phase because its temperatures reach the boiling point of the liquid quench medium. Due to the insulating characteristic of the vapor, heat loss from the probe is limited throughout this phase. Following further cooling, the vapor phase contracts, enabling the probe to interact with the liquid medium, increasing heat loss. The sudden reduction in temperature is caused by the latent heat of the vaporization of the quenchant. It is supplemented by many bubbles erupting from the surface of the quenched probe and collapsing, transferring considerable heat. This period of heat loss is succeeded by convective cooling and occurs due to the reduction of the medium temperature below its boiling point. The heat is transferred from the probe to the liquid medium until it attains uniformity in temperature, causing the rate of heat loss to reduce in the convection stage compared to the nucleate boiling stage. The cooling rate begins slowly and gradually increases until it

https://doi.org/10.1021/acsomega.2c05397
ACS Omega 2022, 7, 47764−47783

Table 2. Values of Temperature and Time for Vapor to Nucleate Boiling Transition for Varying Agitation Rates of Water and Nanofluids

agitation rate (rpm)	type of quench media	t_{A-B} (s)	T_{A-B} (°C)
still	distilled water	4.1	768
	0.02 vol % fullerene	3.1	795
	0.2 vol % fullerene	2.9	800
	0.4 vol % fullerene	2.9	798
	0.0002 vol % TNT	2.8	805
	0.002 vol % TNT	3.3	806
	0.02 vol % TNT	3.7	786
500	distilled water	3.7	778
	0.02 vol % fullerene	3.0	800
	0.2 vol % fullerene	2.5	815
	0.4 vol % fullerene	2.9	801
	0.0002 vol % TNT	3.3	779
	0.002 vol % TNT	3.6	791
	0.02 vol % TNT	4.2	777
1000	distilled water	3.2	763
	0.02 vol % fullerene	2.7	805
	0.2 vol % fullerene	2.2	807
	0.4 vol % fullerene	1.8	820
	0.0002 vol % TNT	2.3	808
	0.002 vol % TNT	3.2	766
	0.02 vol % TNT	3.9	772
1500	distilled water	4.1	716
	0.02 vol % fullerene	2.4	779
	0.2 vol % fullerene	1.6	814
	0.4 vol % fullerene	1.4	825
	0.0002 vol % TNT	2.2	785
	0.002 vol % TNT	2.7	789
	0.02 vol % TNT	4.3	775

reaches a peak value and then decreases with continued cooling progress before the medium and metal probe attain thermal balance. Table 2 shows the temperature (T_{A-B}) and time (t_{A-B}) where the probe center transitioned from the vapor phase to nucleate boiling while quenching with water and nanofluids at varied agitation rates. Compared to distilled water, nanofluids exhibited a higher transition temperature and required less time to shift from the vapor phase to the nucleate boiling stage.[16] It also demonstrates that increasing the agitation rate results in a greater transition temperature and a quicker transition time.

Figures 4 and 5 show that the probe's geometric center during quenching captures critical cooling parameter values retrieved from the cooling rate data presented in Table 2. CR_{max} refers to the maximum cooling rate realized during the quenching process, and Tmax is the temperature at which the quenching process achieves the maximum cooling rate. CR_{700} represents the cooling rate at 700 °C, and at this temperature, the austenite in most steels turns into ferrite, and pearlite takes place. CR_{500} represents the cooling rate at 500 °C. There are numerous plates of steel where the *TTT* curve begins to flatten out at a cooling rate of CR_{550}. A large number of steels undergo martensitic transformations at CR_{300} and CR_{200}. The plots of critical cooling parameters reveal that, at essential temperatures of quenching, nanofluids achieve better cooling rates than water.[17−21] That suggests that nanofluids have a greater hardness when quenched. To examine this behavior, the researchers examined the thermophysical characteristics of the nanofluids.

For water and nanofluids, the thermophysical characteristics are shown in Table 3. The results reveal that the inclusion of fullerene and TNT nanoparticles did not affect the nanofluid viscosity, thermal conductivity, and density. It was found that the surface tension of nanofluids was lower than that of water, with 0.002 vol % TNT having the minimum surface tension and water having the highest surface tension.

The boiling points of nanofluids were investigated to explain the rise in cooling speeds. The boiling point of TNT nanofluids was almost identical to that of pure water (99.5 °C). Fullerene nanofluids had a lower boiling point than water. However, it was only by a few degrees. Nanoparticles were heated to 825 °C in a furnace to check if localized heating during quenching would lead to a phase transition, and it was found that there was no change in phase. Figure 6 depicts contact angle measurements made while a quench medium droplet was dispersed across the Inconel substrate.[22−25] It is apparent from the spreading curves for nanofluids that the contact angle is lowered when nanofluids are added to pure water. Nanofluids with improved wetting on the metal surface are preferable because they help in more even heat extraction than liquids that do not wet well.

Figures 7−12 illustrate the cooling curves near the surface at different axial points undergoing nanofluid quenching. They reveal the changing dynamics of the probe's heat dissipation during quenching. It can be seen from the cooling curves that the liquid medium rewets the probe at various points throughout the quenching process. The liquid quench medium directly contacts the probe when the vapor phase separates. The TC (4) thermocouple has a quicker rewetting time than the other thermocouples, as seen in the graph. As a result, the probe's first point of contact with the liquid medium exhibits more than average heat loss. The existence, formation, and progress of rewetting fronts (loci where the border between the vapor and nucleate boiling phases is created) may be easily observed by the variation in rewetting times measured at different axial positions. Resulting in the significant presence of vaporization, nucleate boiling, and convective cooling phenomena on the probe surface, this rewetting front is accountable for the uneven cooling of the probe.[26−29] The

Table 3. Thermophysical Properties of Water, Fullerene, and TNT Nanofluids

quenchants	density (kg/m^3)	surface tension (MN/m)	viscosity × 10^{-3} (Pa·s)	thermal conductivity (W/m·K)
distilled water	870.3	73	1.34 ± 0.01	0.5845 ± 0.05
0.0002 vol % TNT	871.4	65	1.31 ± 0.01	0.6021 ± 0.03
0.002 vol % TNT	871.5	50	1.33 ± 0.01	0.5804 ± 0.05
0.02 vol % TNT	871.7	60	1.32 ± 0.01	0.5885 ± 0.02
0.02 vol % fullerene	871.5	62	1.31 ± 0.03	0.5587 ± 0.05
0.2 vol % fullerene	871.6	63	1.34 ± 0.01	0.5803 ± 0.04
0.4 vol % fullerene	871.7	63	1.33 ± 0.01	0.6039 ± 0.06

https://doi.org/10.1021/acsomega.2c05397
ACS Omega 2022, 7, 47764−47783

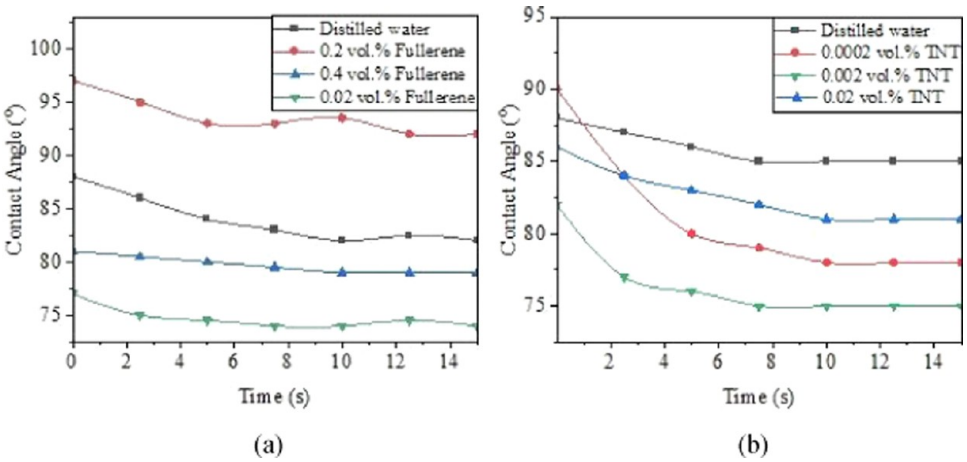

Figure 6. Contact angle relaxation curves for (a) fullerene and (b) TNT nanofluids of various concentrations.

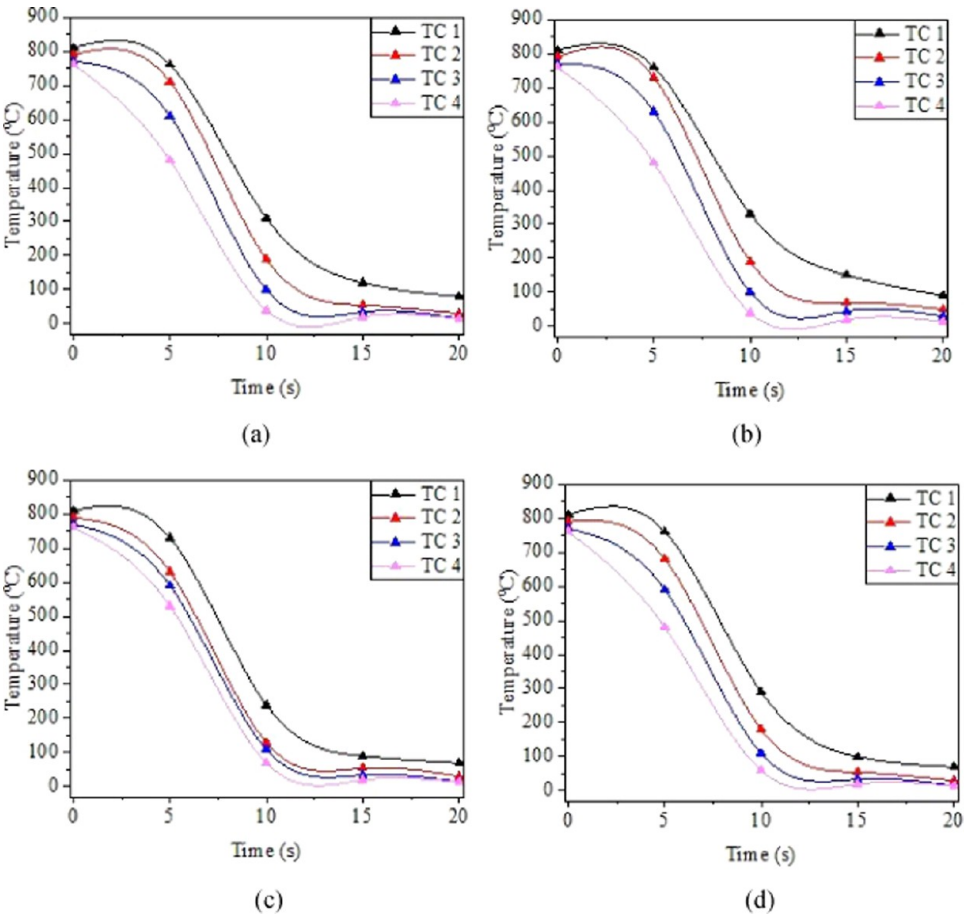

Figure 7. Cooling curves measured at various axial locations in the probe during quenching in the 0.02 vol % fullerene nanofluid under (a) still, (b) 500 rpm, (c) 1000 rpm, and (d) 1500 rpm impeller speeds.

cooling curves show the rapid cooling of the probe to be associated with an increment in the agitation rate of the quench medium.

Figures 13−18 illustrate the interfacial spatiotemporal heat flux following the quenching of TNT and fullerene nanofluids at varying concentrations. Initially, the low heat flux was caused due to the insulating characteristic of the vapor phase that encompassed the probe. Immediately following this delayed phase, the heat flux rises rapidly and decreases as the cooling advances via convection.

Table 4 shows the heat flux peak values for the quench media under varied agitation rates. A higher rate of heat was recovered from the probe when it was agitated in the liquid quench medium. Nanofluids containing 0.02 vol % fullerene had the lowest average peak heat flux (2.55 MW/m^2), whereas nanofluids containing 0.2 vol % fullerene had the most significant average peak heat flux (3.26 MW/m^2). The average peak heat fluxes of other nanofluids were in the middle range. Higher peak heat flux values indicate greater and quicker heat extraction with nanofluids than with water on average. Nayak

https://doi.org/10.1021/acsomega.2c05397
ACS Omega 2022, 7, 47764−47783

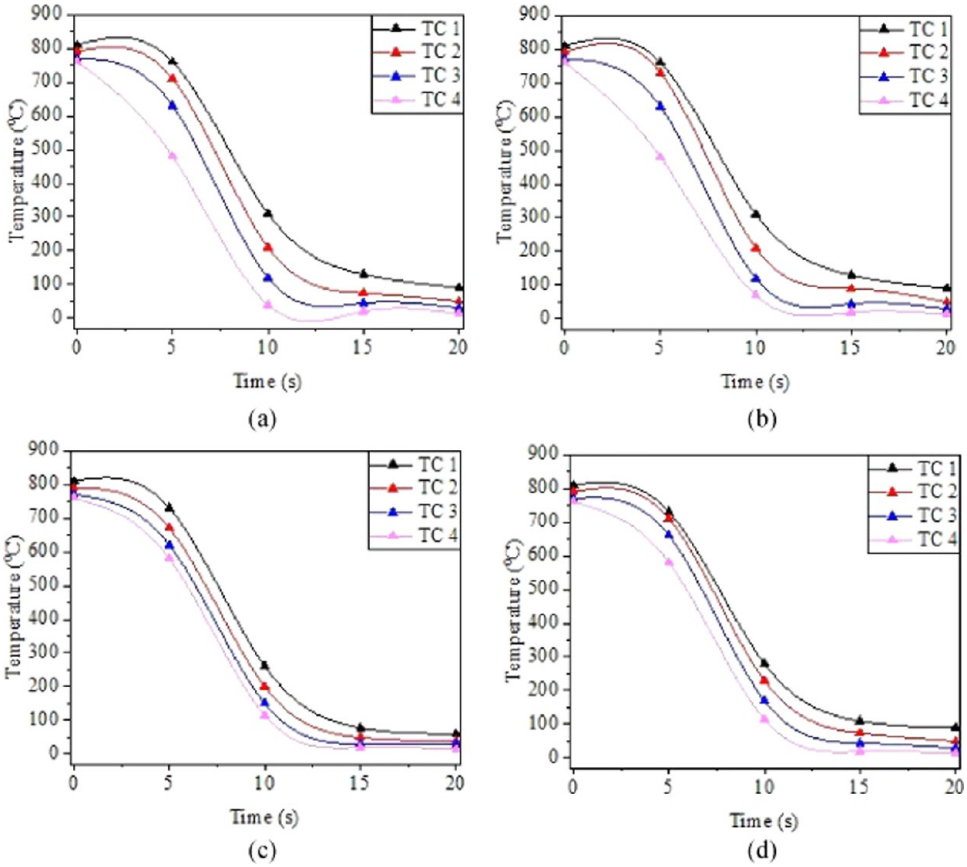

Figure 8. Cooling curves measured at various axial locations in the probe during quenching in the 0.2 vol % fullerene nanofluid under (a) still, (b) 500 rpm, (c) 1000 rpm, and (d) 1500 rpm impeller speeds.

et al. showed a maximum mean heat flux of 3.23 MW/m^2 for the MWCNT nanofluids.[16]

The average heat extraction as a mean surface temperature at 1500 rpm agitation rate for distilled water and TNT nanofluids is shown in Figure 19. These plots were acquired by combining them with the heat flux curves. The average heat extraction plots for TNT demonstrate that at dilute nanoparticle levels of 0.0002 and 0.002 vol %, these nanofluids extract less heat than water as a measure of the mean surface temperature. At a level of 0.02 vol %, the TNT nanofluid extracts higher heat with temperature than water. At all levels, the heat removed by the fullerene nanofluids was somewhat less than that of water. The lower average heat extracted per unit of the mean surface temperature was due to nanofluids extracting heat quicker than water, as seen in Figure 20. It demonstrated conclusively that TNT nanofluids with concentrations of 0.0002 and 0.002 vol % extracted heat quicker than 0.02 vol % TNT and distilled water. This is ascribed to the improved Brownian movement of nanoparticles amid agitated conditions.[30−32] The hydrodynamic interactions generally influence a nanoparticle experiencing Brownian motion in a fluid. The fluid around the particle is dragged in the particle's direction of movement.

Figures 21−24 illustrate the rewetting time and temperature achieved at different agitation settings. The rewetting time and temperature were determined by extracting temperature data from nodes on the surface of the axisymmetric meshed model of the probe that corresponded to the nodes of the near-surface thermocouples (used to take temperature measurements).

These graphs demonstrate that when agitation increased, the time required to rewet the probe decreased, and the rewetting temperatures were greater for nanofluids than water. It is important to note that rewetting occurs when the vapor phase breaks, causing the liquid quench medium to contact the probe. Here, the thermocouple experiences a shorter rewetting time than the other thermocouples. In other words, the probe's location that comes first in contact with the liquid medium shows early heat loss compared to other places.[33-37] The difference in rewetting time observed at various axial locations indicates the formation, existence, and progress of a rewetting front. This rewetting front is responsible for the differential cooling of the probe, leading to differences in the rewetting temperature.

4. CONCLUSIONS

Distilled water and aqueous fullerene nanofluids having concentrations of 0.02, 0.2, and 0.4 vol % and titania (titanium dioxide, TiO_2) nanofluids of 0.0002, 0.002, and 0.02 vol % were analyzed for heat transfer characteristics. The following conclusions have been drawn:

- Unlike distilled water, fullerene and TNT nanofluids possess smaller wetting angles.
- The highest mean heat flux of 3.26 MW/m^2 was obtained for the current study for the fullerene nanofluid of 0.2 vol % concentration under 1500 rpm agitation. That was approximately 10 and 19% greater than the mean peak heat flux for 0.0002 vol % TNT and water, respectively. The higher mean peak heat flux value for

https://doi.org/10.1021/acsomega.2c05397
ACS Omega 2022, 7, 47764−47783

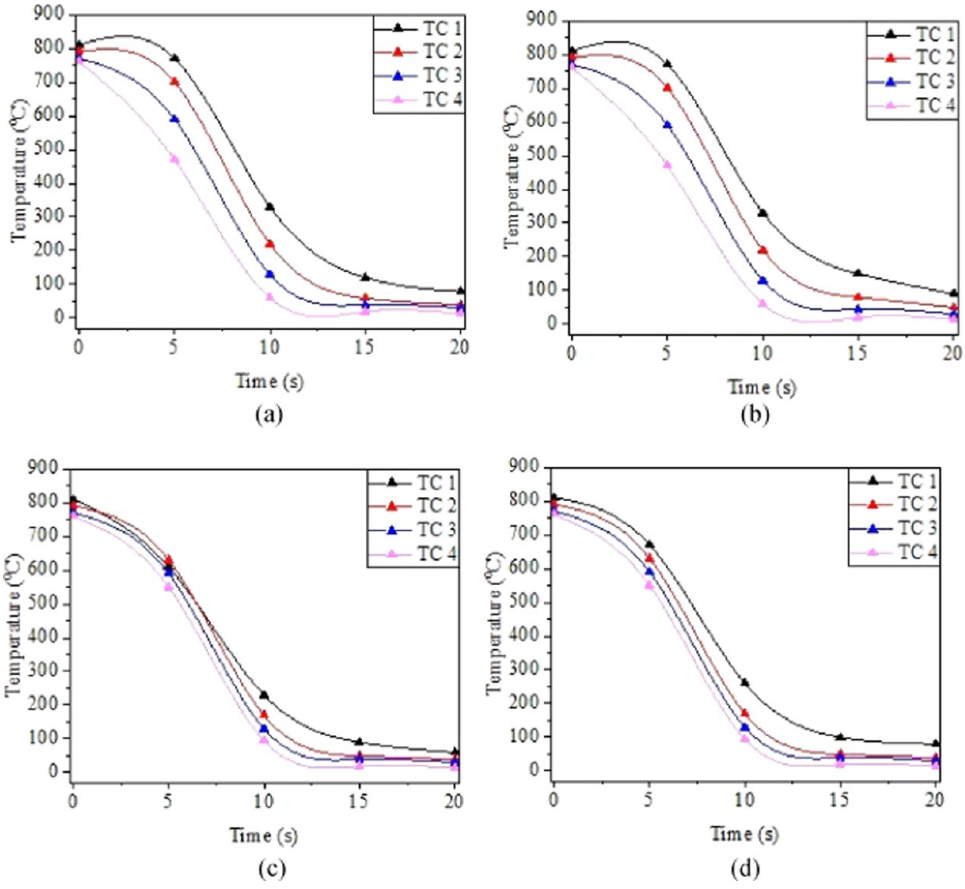

Figure 9. Cooling curves measured at various axial locations in the probe during quenching in 0.4 vol % fullerene nanofluid under (a) still, (b) 500 rpm, (c) 1000 rpm, and (d) 1500 rpm impeller speeds.

nanofluids than water indicates their higher and faster heat extraction capability.

- The quench media characteristics, namely, the viscosity, thermal conductivity, and density of the quench mediums, were all identical. The increased heat flow was due to the accelerated Brownian movement of nanoparticles near the probe wall amid agitated circumstances upon quenching with nanofluids.
- Agitation at 1500 rpm significantly reduced the rewetting time for fullerene nanofluids, with a 57% decrease in quenching with the 0.2 vol % fullerene nanofluid compared to the still quench condition. This was mainly due to the simultaneous occurrence of vapor, nucleate boiling, and convective cooling heat transfer mechanisms on the surface of the probe. The corresponding decreases were approximately 31 and 11% upon quenching with the 0.0002 vol % TNT nanofluid and water, respectively.

AUTHOR INFORMATION

Corresponding Authors

Jaimon Dennis Quadros − *Faculty of Mechanical Engineering, Istanbul Technical University, 34437 İstanbul, Turkey*; Email: jaimonq@gmail.com

Saboor Shaik − *School of Mechanical Engineering, Vellore Institute of Technology, Vellore 632014 Tamil Nadu, India*; orcid.org/0000-0002-0490-4766; Email: saboor.nitk@gmail.com

Authors

Sher Afghan Khan − *Department of Mechanical Engineering, Faculty of Engineering, International Islamic University Malaysia, Kuala Lumpur 53100 Selangor, Malaysia*

Prashanth T − *Department of Mechanical Engineering, Global Academy of Technology, Bengaluru 560098 Karnataka, India*

Yakub Iqbal Mogul − *National Centre for Motorsport Engineering, University of Bolton, Bolton BL3 5AB, U.K.*

Hanumanthraya R − *School of Mechanical Engineering, REVA University, Bengaluru 560064 Karnataka, India*

Mohamed Abbas − *Electrical Engineering Department, College of Engineering, King Khalid University, Abha 61421, Saudi Arabia; Electronics and communications Department, College of Engineering, Delta University for Science and Technology, Mansoura 35712, Egypt*

C. Ahamed Saleel − *Department of Mechanical Engineering, College of Engineering, King Khalid University, Abha 61421, Saudi Arabia*

Complete contact information is available at: https://pubs.acs.org/10.1021/acsomega.2c05397

Notes

The authors declare no competing financial interest.

ACKNOWLEDGMENTS

The authors thank the Deanship of Scientific Research at King Khalid University, Saudi Arabia, for funding this work through

https://doi.org/10.1021/acsomega.2c05397
ACS Omega 2022, 7, 47764−47783

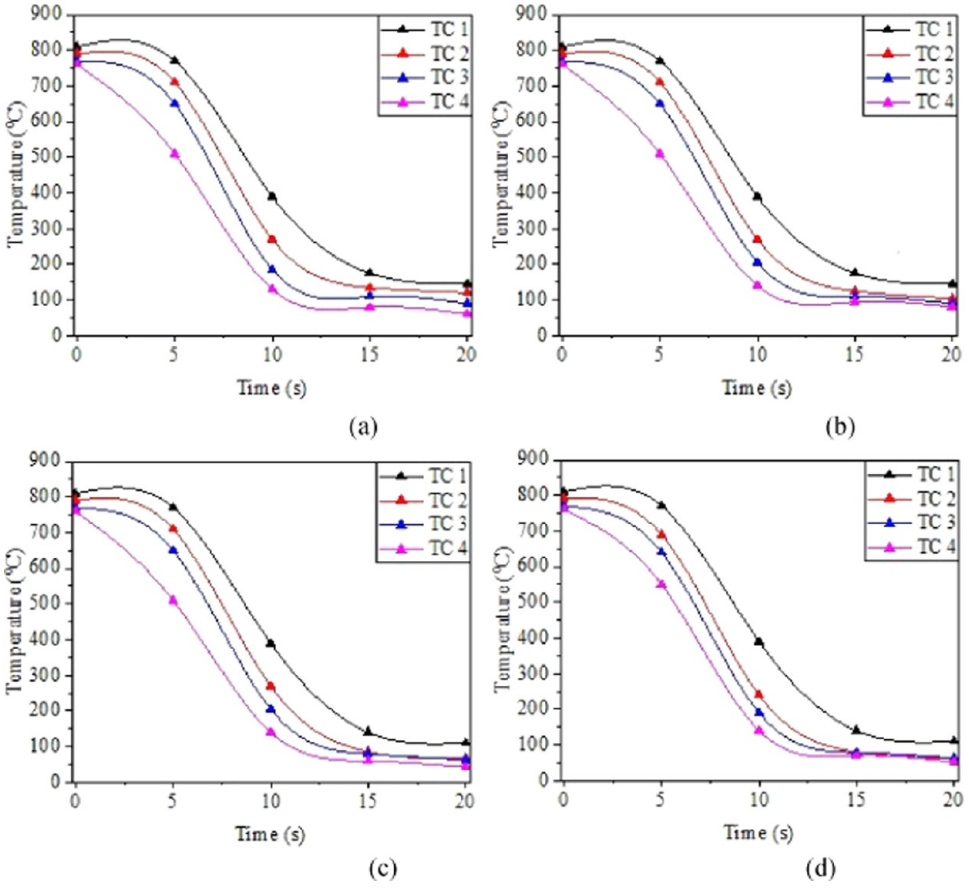

Figure 10. Cooling curves measured at various axial locations in the probe during quenching in the 0.0002 vol % TNT nanofluid under (a) still, (b) 500 rpm, (c) 1000 rpm, and (d) 1500 rpm impeller speeds.

the Research Group Program under Grant No: R.G.P. 1/256/43.

REFERENCES

(1) French, H. J.; Hamill, T. E. Hot aqueous solutions for the quenching of steels. *Bur. Stand. J. Res.* **1929**, *3*, 399−418.

(2) Ramesh, G.; Prabhu, K. N. Review of thermo-physical properties, wetting and heat transfer characteristics of nanofluids and their applicability in industrial quench heat treatment. *Nanoscale Res. Lett.* **2011**, *6*, No. 334.

(3) Kim, H.; DeWitt, G.; McKrell, J. T.; Buongiorno, J.; Hu, L. W. On the quenching of steel and zircaloy spheres in water-based nanofluids with alumina, silica and diamond nanoparticles. *Int. J. Multiphase Flow* **2009**, *35*, 427−438.

(4) Ciloglu, D.; Bolukbasi, A. The quenching behavior of aqueous nanofluids around rods with high temperature. *Nucl. Eng. Des.* **2011**, *241*, 2519−2527.

(5) Schauperl, Z.; Solic, S. In *MATRIB*, International Conference on Materials, Tribology, Recycling; Vela Luka: Croatia, 2011.

(6) Babu, K.; Kumar, T. S. P. Effect of CNT concentration and agitation on surface heat flux during quenching in CNT nanofluids. *Int. J. Heat Mass Transfer* **2011**, *54*, 106−117.

(7) MacKenzie, D. S. In *Quench Control and Distortion*, Proceedings from 6th International Conferenceon Quenching Control Distortion Conf. Incl. 4th International distortion Engineering Conference; ASM International: Chicago, USA, 2012.

(8) Howson, M. P.; Wynne, B. P.; Mercado-Solis, R. D.; Leduc-Lezama, L. A.; Jonny, J.; Shaji, S. An Analysis of the Quenching Performance of a Copper Nanofluid Prepared Using Laser Ablation. *J. Therm. Sci. Eng. Appl.* **2016**, *8*, No. 044501.

(9) Afzal, A.; Khan, S. A.; Saleel, C. A. Role of ultrasonication duration and surfactant on characteristics of ZnO and CuO nanofluids. *Mater. Res. Express* **2019**, *6*, No. 1150d8.

(10) Wlazlak, A.; Zajaczkowski, B.; Woluntarski, M.; Buschmann, M. H. Influence of graphene oxide nanofluids and surfactant on thermal behaviour of the thermosyphon. *J. Therm. Anal. Calorim.* **2019**, *136*, 843−855.

(11) Saleh, B.; Sundar, L. S.; Aly, A. A.; Ramana, V. E.; Sharma, K. V.; Afzal, A.; Abdelrahman, Y.; Sousa, C. M. A. The Combined Effect of Al_2O_3 Nanofluid and Coiled Wire Inserts in a Flat-Plate Solar Collector on Heat Transfer, Thermal Efficiency and Environmental CO_2 Characteristics. *Arabian J. Sci. Eng.* **2022**, *47*, 9187−9214.

(12) Afzal, A.; Samee, A. D.; Razak, R. K. A.; Ramis, M. K. Heat transfer characteristics of MWCNT nanofluid in rectangular mini channels. *Int. J. Heat Technol.* **2017**, *36*, 222−228.

(13) Samylingam, L.; Aslfattahi, N.; Saidur, R.; Yahya, S. M.; Afzal, A.; Arifutzzaman, A.; Tan, K. H.; Kadirgama, K. Thermal and energy performance improvement of hybrid PV/T system by using olein palm oil with MXene as a new class of heat transfer fluid. *Sol. Energy Mater. Sol. Cells* **2020**, *218*, No. 110754.

(14) Younes, H.; Mao, M.; Murshed, S. M. S.; Lou, D.; Hong, H.; Peterson, G. P. Nanofluids: Key parameters to enhance thermal conductivity and its applications. *App. Therm. Eng.* **2022**, *207*, No. 118202.

(15) Kumar, T. S. A serial solution for the 2-D inverse heat conduction problem for estimating multiple heat flux components. *Numer. Heat Transfer, Part B* **2004**, *45*, 541−563.

(16) Nayak, U. V.; Prabhu, K. N. Heat Transfer During Quenching in Graphene and Multiwall Carbon Nanotubes Nanofluids Under Agitated Quench Conditions. *J. Nanofluids* **2019**, *8*, 1222−1239.

https://doi.org/10.1021/acsomega.2c05397
ACS Omega 2022, 7, 47764−47783

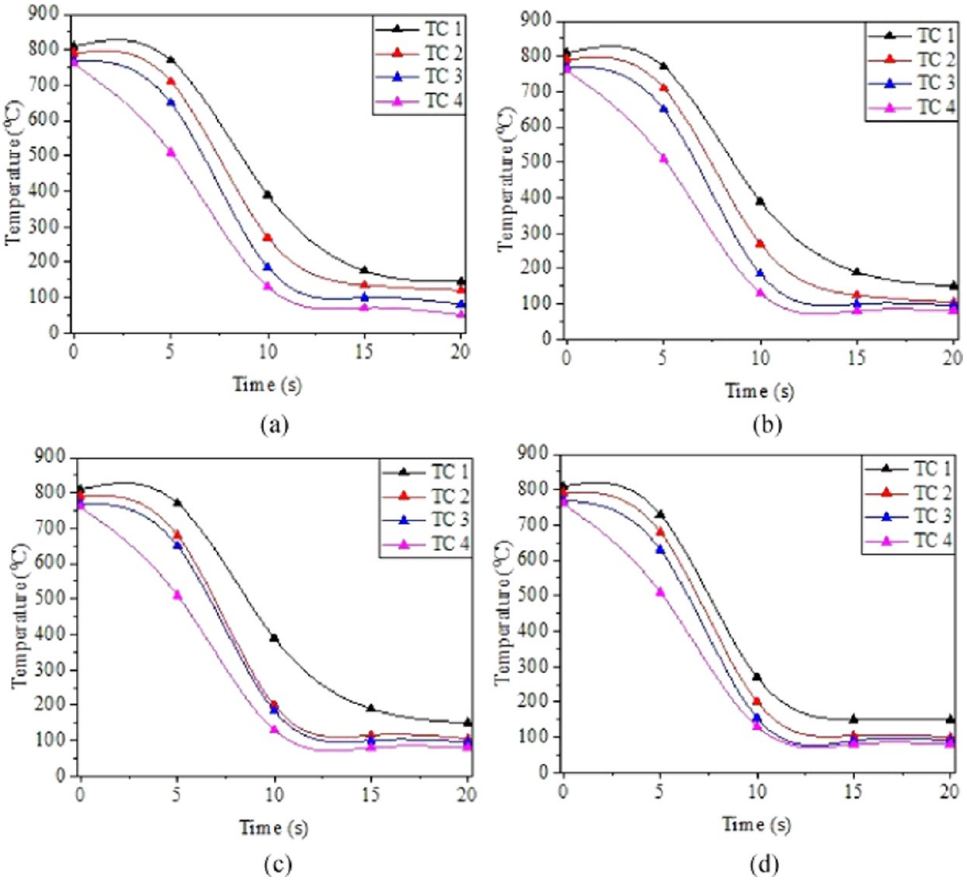

Figure 11. Cooling curves measured at various axial locations in the probe during quenching in the 0.002 vol % TNT nanofluid under (a) still, (b) 500 rpm, (c) 1000 rpm, and (d) 1500 rpm impeller speeds.

(17) Yashawantha, K. M.; Asif, A.; Babu, G. R.; Ramis, M. K. Rheological Behavior and Thermal Conductivity of Graphite−Ethylene Glycol Nanofluid. *J. Test. Eval.* **2019**, *49*, No. 20190255.
(18) Kareemullah, M.; Afzal, A.; Rehman, K. F.; Shahapurkar, K.; Khan, H.; Akram, N. Performance and Emission Analysis of Compression Ignition Engine Using Biodiesels from Acid Oil, Mahua Oil, and Castor Oil. *Heat Transfer* **2020**, *49*, 858−871.
(19) Afzal, A.; Nawfal, I.; Mahbubul, I. M.; Kumbar, S. S. An Overview on the Effect of Ultrasonication Duration on Different Properties of Nanofluids. *J. Therm. Anal. Calorim.* **2019**, *135*, 393−418.
(20) Dhairiyasamy, R.; Saleh, B.; Govindasamy, M.; Aly, A. A.; Afzal, A.; Abdelrhman, Y. Effect of Particle Size on Thermophysical and Heat Transfer Properties of Ag Nanofluid in a Radiator−an Experimental Investigation. *Inorg. Nano-Met. Chem.* **2021**, 1−15.
(21) Afzal, A.; Islam, M. T.; Kaladgi, A. R.; Manokar, A. M.; Samuel, O. D.; Mujtaba, M. A.; Soudagar, M. E. M.; Fayaz, H.; Ali, H. M. Experimental Investigation on the Thermal Performance of Inserted Helical Tube Three-Fluid Heat Exchanger Using Graphene/Water Nanofluid. *J. Therm. Anal. Calorim.* **2021**, *147*, 5087−5100.
(22) Ağbulut, Ü.; Sarıdemir, S.; Rajak, U.; Polat, F.; Afzal, A.; Verma, T. N. Effects of High-Dosage Copper Oxide Nanoparticles Addition in Diesel Fuel on Engine Characteristics. *Energy* **2021**, *229*, No. 120611.
(23) Saleh, B.; Sundar, L. S.; Aly, A. A.; Ramana, E. V.; Sharma, K. V.; Afzal, A.; Abdelrhman, Y.; Sousa, A. C. M. The Combined Effect of Al2O3 Nanofluid and Coiled Wire Inserts in a Flat-Plate Solar Collector on Heat Transfer, Thermal Efficiency and Environmental CO2 Characteristics. *Arabian J. Sci. Eng.* **2022**, *47*, 9187−9214.
(24) Afzal, A.; Yashawantha, K. M.; Aslfattahi, N.; Saidur, R.; Razak, R. K. A.; Subbiah, R. Back Propagation Modeling of Shear Stress and Viscosity of Aqueous Ionic - MXene Nanofluids. *J. Therm. Anal. Calorim.* **2021**, *145*, 2129−2149.
(25) Mujtaba, M. A.; Muk Cho, H.; Masjuki, H. H.; Kalam, M. A.; Farooq, M.; Soudagar, M. E. M.; Gul, M.; Ahmed, W.; Afzal, A.; Bashir, S.; et al. Effect of Alcoholic and Nano-Particles Additives on Tribological Properties of Diesel−Palm−Sesame−Biodiesel Blends. *Energy Rep.* **2020**, *7*, 1162−1171.
(26) Hussain, F.; Soudagar, M. E. M.; Afzal, A.; Mujtaba, M. A.; Badruddin, I. A.; Khan, T. M. Y.; Raju, V. D.; Gavhane, R. S.; Rahman, S. M. A.; et al. Enhancement in Combustion, Performance, and Emission Characteristics of a Diesel Engine Fueled with Ce-ZnO Nanoparticle Additive Added to Soybean Biodiesel Blends. *Energies* **2020**, *13*, No. 4578.
(27) Said, Z.; Sharma, P.; Sundar, L. S.; Afzal, A.; Li, C. Synthesis, Stability, Thermophysical Properties and AI Approach for Predictive Modelling of Fe3O4 Coated MWCNT Hybrid Nanofluids. *J. Mol. Liq.* **2021**, *340*, No. 117291.
(28) Ziaee, O.; Zolfaghari, N.; Baghani, M.; Baniassadi, M.; Wang, K. A modified cellular automaton model for simulating ion dynamics in a Li-ion battery electrode. *Energy Equip. Syst.* **2022**, *10*, 41−49.
(29) Taslimi, M. S.; Dastjerdi, S. M.; Mousavi, S. B.; Ahmadi, P.; Ashjaee, M. Assessment and multi-objective optimization of an off-grid solar based energy system for a Conex. *Energy Equip. Syst.* **2021**, *9*, 127−143.
(30) Sharifi, M.; Amidpour, M.; Mollaei, S. Investigating carbon emission abatement long-term plan with the aim of energy system modeling; case study of Iran. *Energy Equip. Syst.* **2018**, *6*, 337−349.
(31) Zare, S.; Ayati, M.; Ha'iri Yazdi, M. R.; Kabir, A. A. Convolutional neural networks for wind turbine gearbox health monitoring. *Energy Equip. Syst.* **2022**, *10*, 73−82.

https://doi.org/10.1021/acsomega.2c05397
ACS Omega 2022, 7, 47764−47783

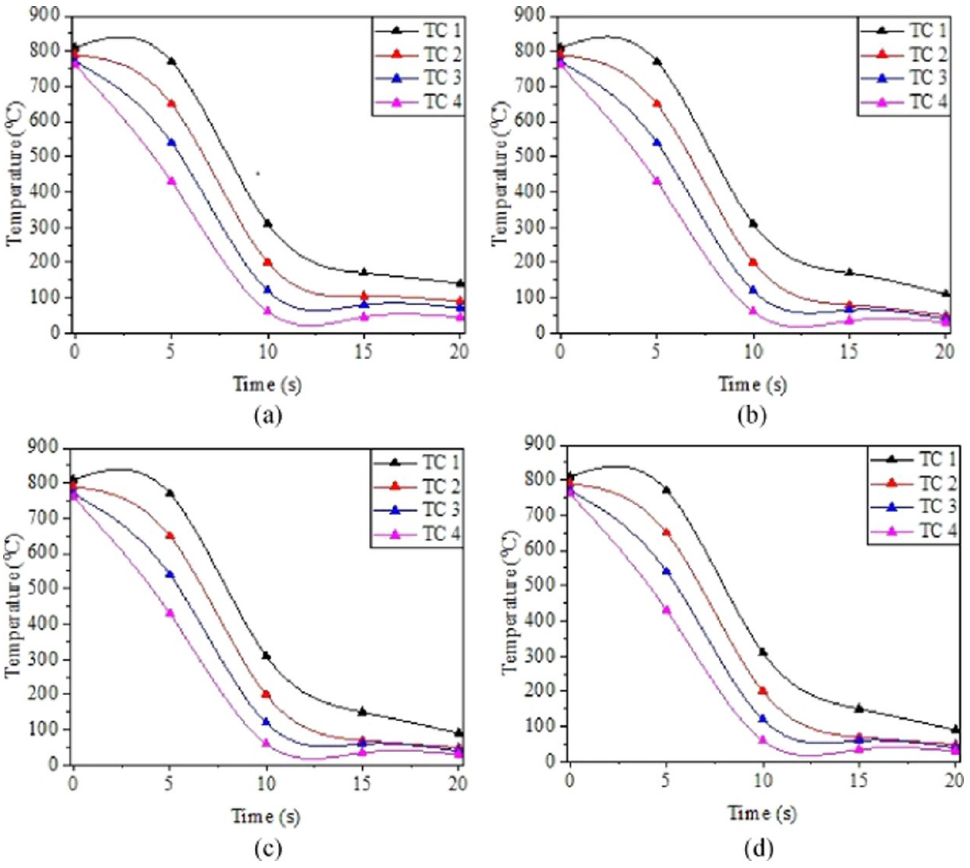

Figure 12. Cooling curves measured at various axial locations in the probe during quenching in the 0.02 vol % TNT nanofluid under (a) still, (b) 500 rpm, (c) 1000 rpm, and (d) 1500 rpm impeller speeds.

(32) Sabzi, S.; Asadi, M.; Moghbelli, H. Review, analysis and simulation of different structures for hybrid electrical energy storages. *Energy Equip. Syst.* **2017**, *5*, 115−129.

https://doi.org/10.1021/acsomega.2c05397
ACS Omega 2022, 7, 47764−47783

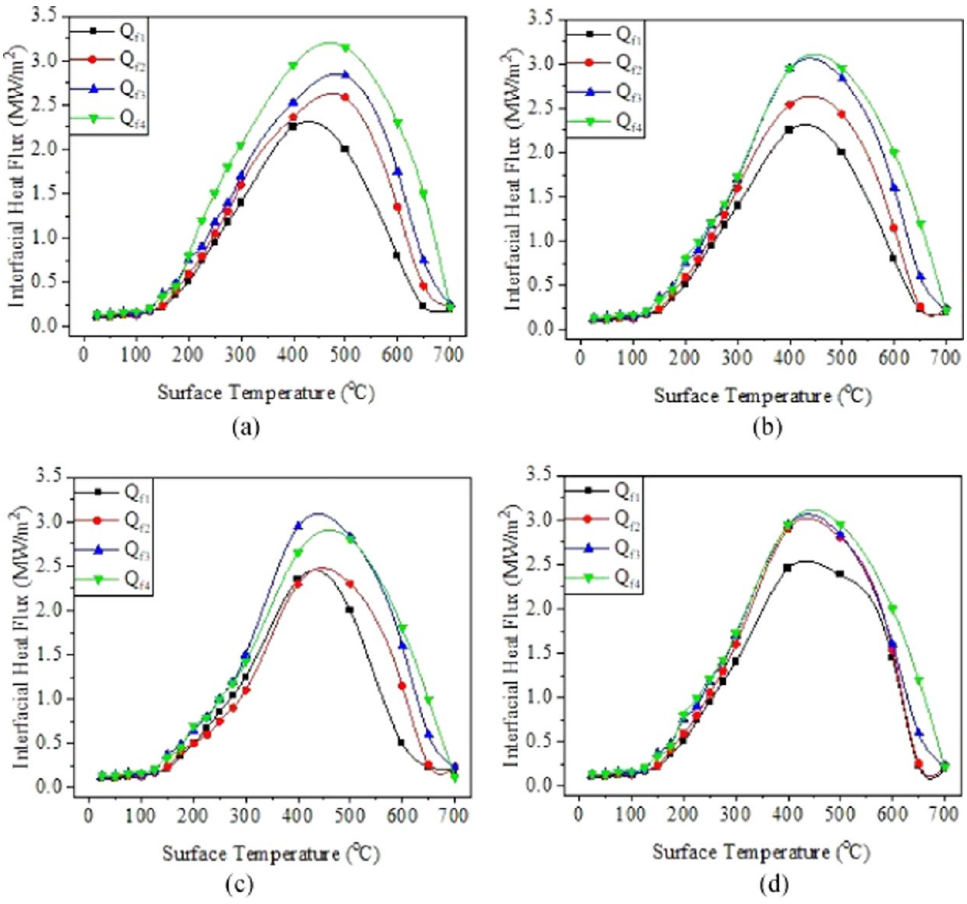

Figure 13. Cooling curves measured at various axial locations in the probe during quenching in the 0.02 vol % fullerene nanofluid under (a) still, (b) 500 rpm, (c) 1000 rpm, and (d) 1500 rpm impeller speeds.

https://doi.org/10.1021/acsomega.2c05397
ACS Omega 2022, 7, 47764−47783

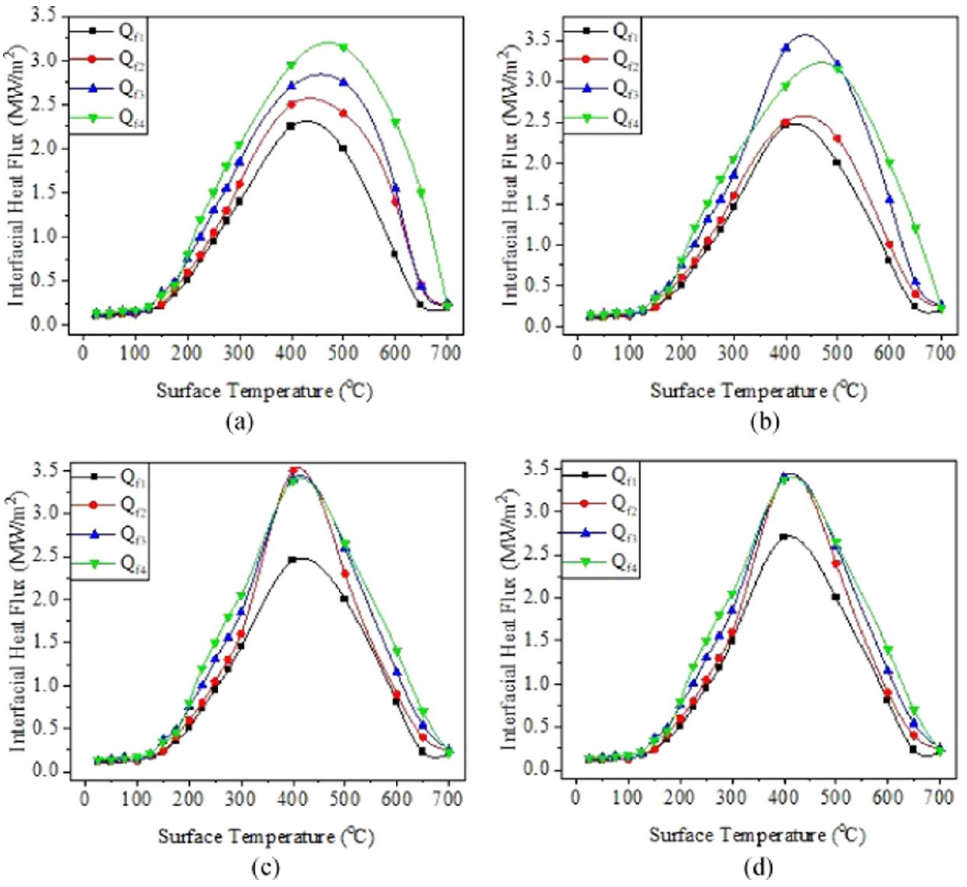

Figure 14. Cooling curves measured at various axial locations in the probe during quenching in the 0.2 vol % fullerene nanofluid under (a) still, (b) 500 rpm, (c) 1000 rpm, and (d) 1500 rpm impeller speeds.

https://doi.org/10.1021/acsomega.2c05397
ACS Omega 2022, 7, 47764−47783

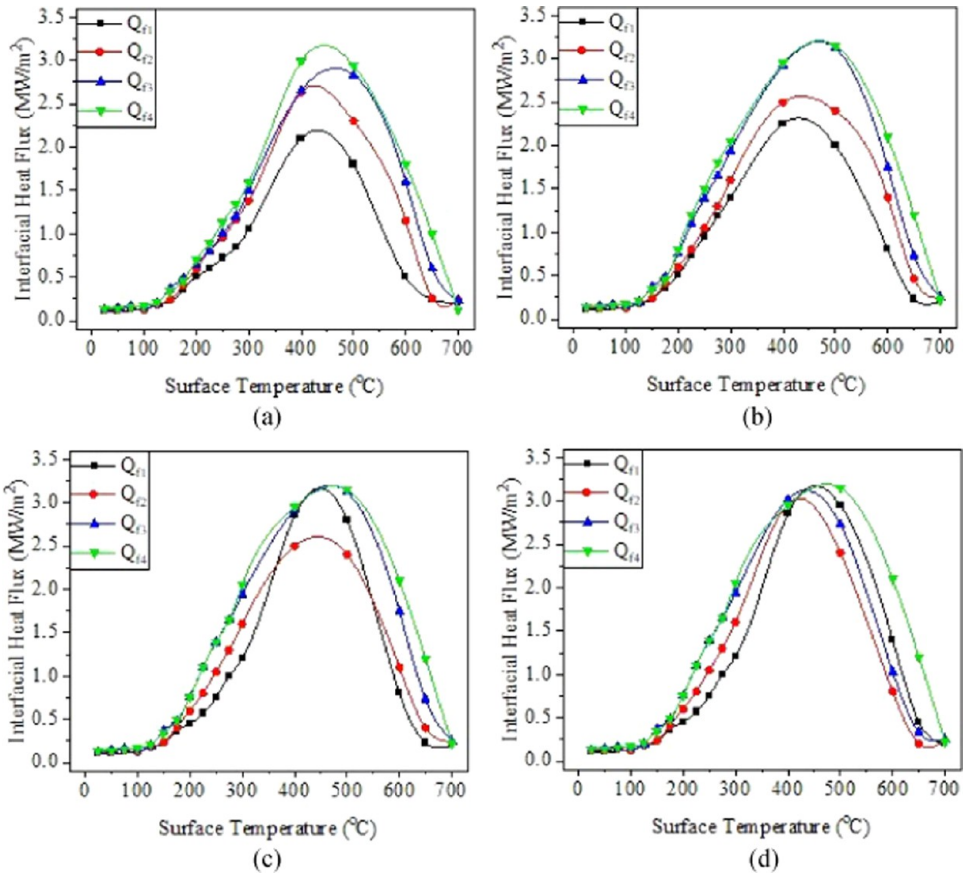

Figure 15. Cooling curves measured at various axial locations in the probe during quenching in the 0.4 vol % fullerene nanofluid under (a) still, (b) 500 rpm, (c) 1000 rpm, and (d) 1500 rpm impeller speeds.

https://doi.org/10.1021/acsomega.2c05397
ACS Omega 2022, 7, 47764−47783

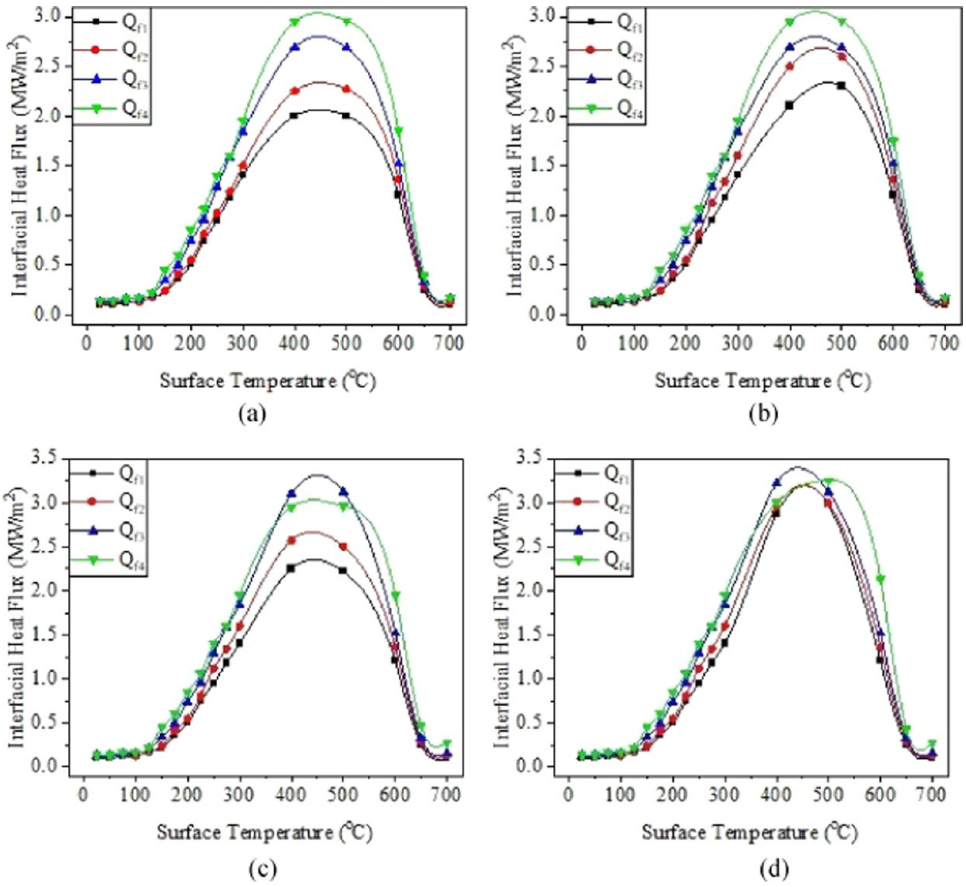

Figure 16. Cooling curves measured at various axial locations in the probe during quenching in the 0.0002 vol % TNT nanofluid under (a) still, (b) 500 rpm, (c) 1000 rpm, and (d) 1500 rpm impeller speeds.

https://doi.org/10.1021/acsomega.2c05397
ACS Omega 2022, 7, 47764−47783

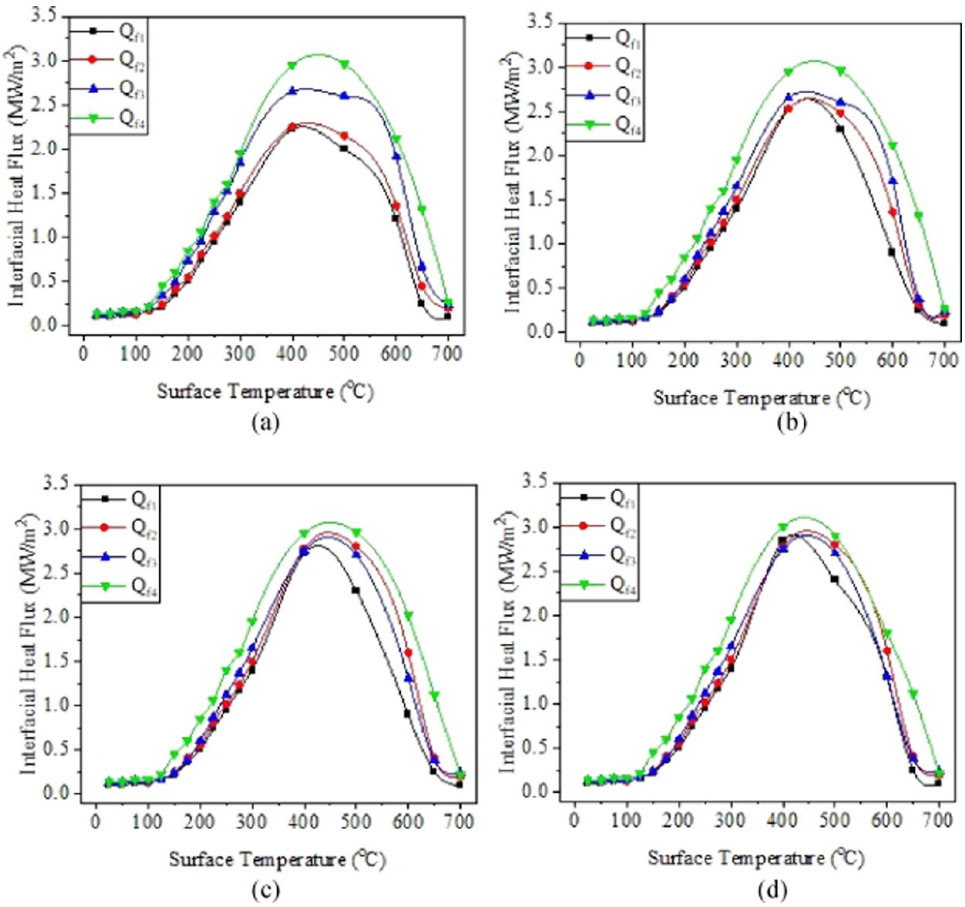

Figure 17. Cooling curves measured at various axial locations in the probe during quenching in the 0.002 vol % TNT nanofluid under (a) still, (b) 500 rpm, (c) 1000 rpm, and (d) 1500 rpm impeller speeds.

https://doi.org/10.1021/acsomega.2c05397
ACS Omega 2022, 7, 47764−47783

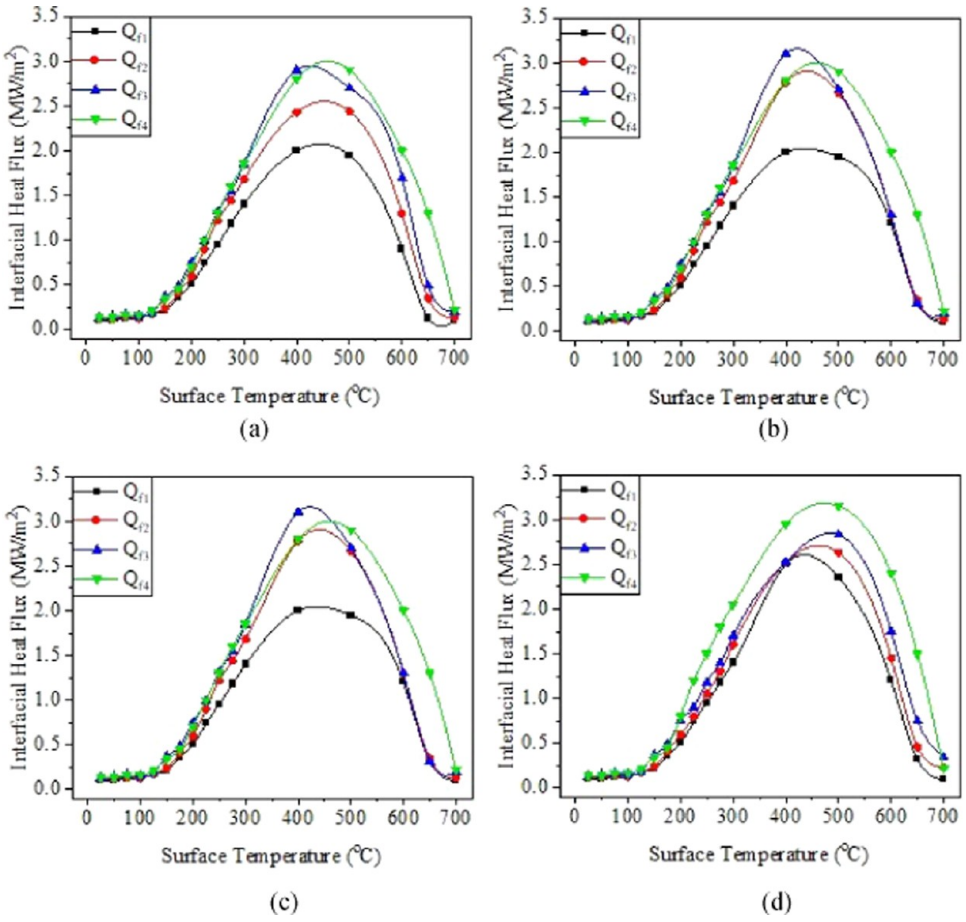

Figure 18. Cooling curves measured at various axial locations in the probe during quenching in the 0.02 vol % TNT nanofluid under (a) still, (b) 500 rpm, (c) 1000 rpm, and (d) 1500 rpm impeller speeds.

https://doi.org/10.1021/acsomega.2c05397
ACS Omega 2022, 7, 47764−47783

Table 4. Heat Flux Values for Quenching

		top half		bottom half			
agitation rate (rpm)	type of quench media	Q_{f1}	Q_{f2}	Q_{f3}	Q_{f4}	average	standard deviation
still	distilled water	1.97	2.87	2.45	2.80	2.59	0.41
	0.0002 vol % TNT	2.25	2.60	2.99	3.09	2.73	0.30
	0.002 vol % TNT	2.10	2.45	2.68	2.95	2.55	0.36
	0.02 vol % TNT	2.02	2.47	2.94	2.90	2.58	0.43
	0.02 vol % fullerene	1.95	2.52	2.69	3.03	2.55	0.45
	0.2 vol % fullerene	1.84	2.69	2.97	3.11	2.65	0.57
	0.4 vol % fullerene	1.90	2.57	2.85	3.06	2.60	0.50
500	distilled water	2.44	2.56	2.78	2.76	2.64	0.16
	0.0002 vol % TNT	2.12	2.72	3.02	3.22	2.77	0.48
	0.002 vol % TNT	2.58	2.65	2.71	3.25	2.80	0.31
	0.02 vol % TNT	2.12	2.80	2.99	2.89	2.70	0.39
	0.02 vol % fullerene	2.20	2.85	3.05	3.17	2.82	0.43
	0.2 vol % fullerene	2.65	2.92	3.39	3.31	3.07	0.35
	0.4 vol % fullerene	2.50	2.89	3.10	3.14	2.91	0.29
1000	distilled water	2.50	2.90	2.99	3.05	2.86	0.25
	0.0002 vol % TNT	2.46	2.75	3.22	3.10	2.88	0.35
	0.002 vol % TNT	2.65	2.99	2.95	3.28	2.97	0.26
	0.02 vol % TNT	2.39	2.60	2.55	2.88	2.61	0.20
	0.02 vol % fullerene	2.55	2.68	3.48	3.11	2.96	0.42
	0.2 vol % fullerene	2.61	3.21	3.22	3.20	3.06	0.30
	0.4 vol % fullerene	2.90	2.91	3.28	3.25	3.09	0.21
1500	distilled water	2.60	2.92	2.58	2.98	2.77	0.21
	0.0002 vol % TNT	2.70	2.99	3.20	3.10	3.00	0.21
	0.002 vol % TNT	2.81	3.07	2.98	3.12	3.00	0.14
	0.02 vol % TNT	2.52	3.05	2.66	3.03	2.82	0.27
	0.02 vol % fullerene	2.58	3.04	3.00	3.20	2.96	0.26
	0.2 vol % fullerene	2.81	3.35	3.40	3.48	3.26	0.30
	0.4 vol % fullerene	2.99	2.95	3.26	3.31	3.13	0.18

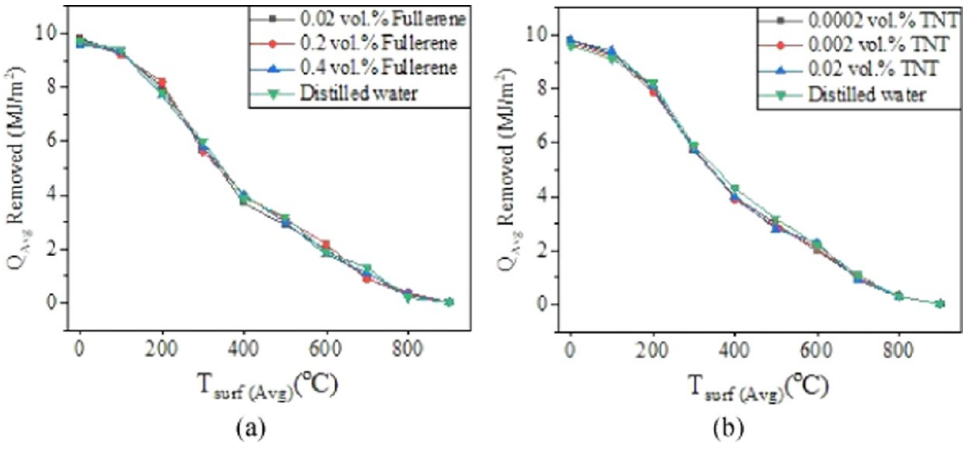

Figure 19. Average heat removed vs the average surface temperature obtained during quenching with (a) fullerene and (b) TNT nanofluids of various concentrations at an impeller rotation rate of 1500 rpm.

https://doi.org/10.1021/acsomega.2c05397
ACS Omega 2022, 7, 47764−47783

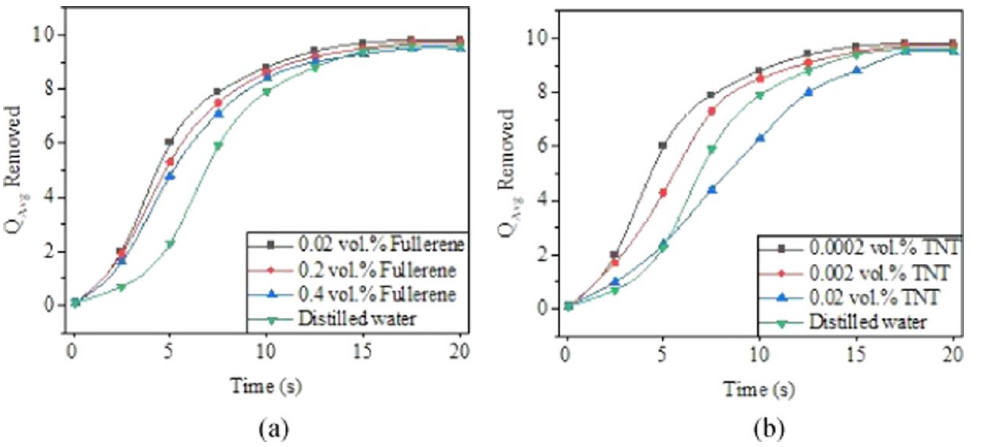

Figure 20. Average heat removed vs time obtained during quenching with (a) fullerene and (b) TNT nanofluids of various concentrations at an impeller rotation rate of 1500 rpm.

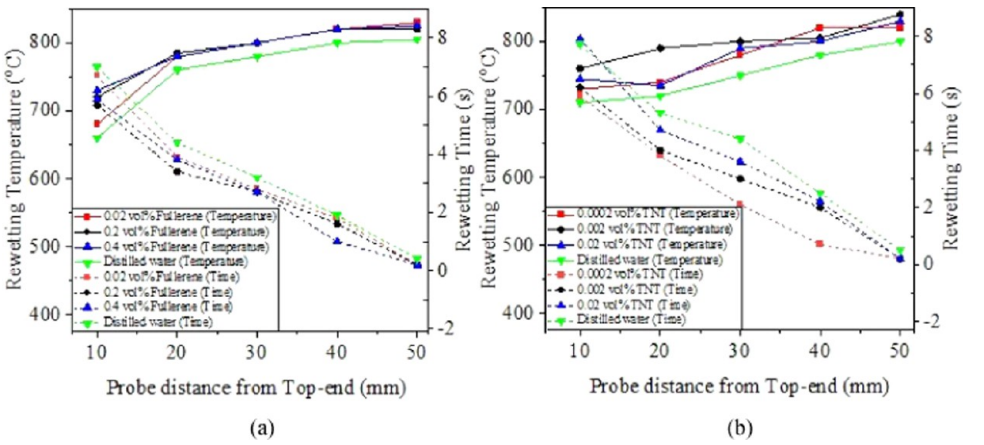

Figure 21. Rewetting time and rewetting temperature with respect to the probe distance obtained with (a) distilled water and 0.02, 0.2, and 0.4 vol % fullerene nanofluids and (b) distilled water and 0.0002, 0.002, and 0.02 vol % TNT nanofluids under still agitation rates.

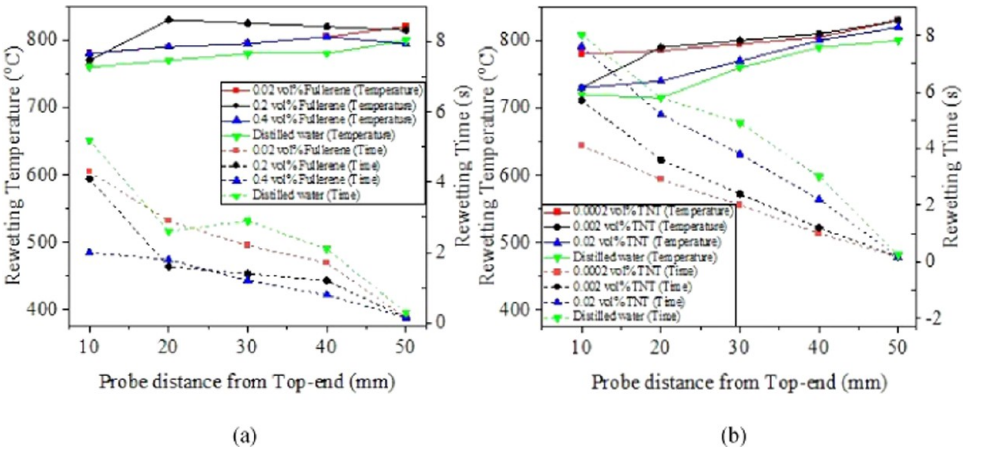

Figure 22. Rewetting time and rewetting temperature with respect to the probe distance obtained with (a) distilled water and 0.02, 0.2, and 0.4 vol % fullerene nanofluids and (b) distilled water and 0.0002, 0.002, and 0.02 vol % TNT nanofluids under 500 rpm agitation rates.

https://doi.org/10.1021/acsomega.2c05397
ACS Omega 2022, 7, 47764−47783

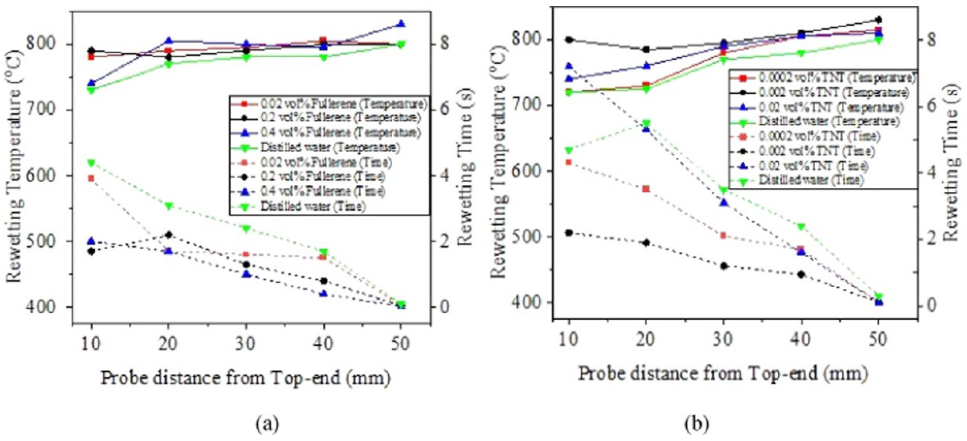

Figure 23. Rewetting time and rewetting temperature with respect to the probe distance obtained with (a) distilled water and 0.02, 0.2, and 0.4 vol % fullerene nanofluids and (b) distilled water and 0.0002, 0.002, and 0.02 vol % TNT nanofluids under 1000 rpm agitation rates.

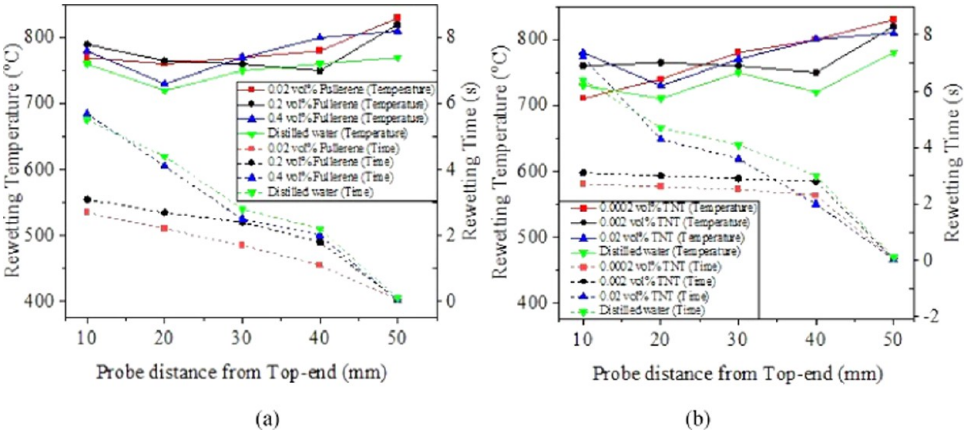

Figure 24. Rewetting time and rewetting temperature with respect to the probe distance obtained with (a) distilled water and 0.02, 0.2, and 0.4 vol % fullerene nanofluids and (b) distilled water and 0.0002, 0.002, and 0.02 vol % TNT nanofluids under 1500 rpm agitation rates.

https://doi.org/10.1021/acsomega.2c05397
ACS Omega 2022, 7, 47764−47783